


 Cite this: *Chem. Commun.*, 2023, 59, 8412

 Received 13th April 2023,
Accepted 9th June 2023

DOI: 10.1039/d3cc01818k

rsc.li/chemcomm

Molecular unravelling of the mechanism of overpotential change at the carbon nanotubes-modified gold electrode surface†

 Yanyan Zhang,^{id} ^a Jing Jin,^{ac} Yifei Xue,^b Yao Zhao,^{id} ^a Qun Luo,^{ac}
Lanqun Mao,^{id} ^{ab} and Fuyi Wang,^{id} ^{*ac}

Using liquid secondary ion mass spectrometry, we *in situ* unraveled that the single walled carbon nanotubes-modified gold electrode surface is free of a dense adsorption phase and abundant in water molecules, which facilitated the electro-oxidation reaction of ascorbate. Such an understanding will expedite the knowledge-based development of electrochemical interfaces.

The electrode–electrolyte interface is central to all electrochemical processes, the chemical structure of which governs its properties and determines the reaction dynamics and mechanism. Owing to their excellent electrical conductivity and high specific surface area, carbon materials such as carbon nanotubes (CNTs),^{1–7} graphene^{3,4,7–9} and graphdiyne^{10–16} have attracted extensive attention to advance electrode–electrolyte interfaces such as lowering the overpotential to drive down the energy costs. The overpotential is the additional potential beyond the thermodynamic requirement to drive a reaction at a certain rate.¹⁷ To date, the fundamental understanding of the origin of the overpotential as well as the mechanism of the lowered overpotential by carbon materials modification is limited. This is due to the lack of suitable *in situ* and *operando* techniques that allow a direct access to the molecular structures of carbon materials-modified electrochemical interfaces and their link with the interface reactions. Traditional *in situ* characterization methods such as infrared reflection adsorption spectroscopy (IRAS) and surface enhanced Raman spectroscopy (SERS) can provide valuable information on the local bonding and orientation of species near the interfaces.^{18–20} Whereas, there exist challenges for these techniques to tackle with the carbon materials-modified interfacial chemistry which arise from either serious absorption of infrared energy by

carbon materials or the difficulty to amplify contribution of species at such interfaces by plasmonic enhancement. Another major limitation of using these vibrational spectroscopic techniques is that direct observation of simple cations in electrolytes such as alkali cations is not possible, blocking the unveiling of a comprehensive picture of interfacial structures.

In our recent studies, an electrochemical liquid secondary ion mass spectrometry (SIMS) technique was developed by interfacing a home-made high-vacuum-compatible electrochemical device with SIMS and has been established as a robust toolkit for *in situ* and *operando* probing of electrochemical interfaces.^{21–25} The key of this technique is a tiny aperture formed by the analysis ion beam on the silicon nitride membrane window on top of the electrochemical device, through which the beam could *in situ* bombard and probe the underneath electrode–electrolyte interface under *operando* conditions. Due to the relatively soft ionization process,^{26,27} high surface sensitivity^{21,25} and no bias for detection of cations and anions,^{25,28} the electrochemical liquid SIMS has provided direct molecular evidences of chemical distributions within electrical double layer structures^{21,24,25} as well as electrochemical/electrocatalytic reaction mechanisms^{21–23,25} at the metallic electrode–electrolyte interfaces.

Herein, we report a molecular investigation of whether and how modification of single walled carbon nanotubes (SWCNTs) on a gold electrode surface alters the electrochemical interfacial chemistry as a case study by a tailored electrochemical liquid SIMS platform. We unraveled that the gold electrode surface in a phosphate buffer suffered from a dense adsorption phase formed of cation–anion interactions which seriously retarded the access of electrochemically active species. In sharp contrast, the SWCNTs modification on the gold electrode surface significantly tuned the interfacial structures to be free of the adsorption phase and much more abundant in water molecules, which promoted both the electron transfer and proton transfer during the proton coupled electrochemical oxidation of ascorbate. This work provides an unprecedented molecular understanding of the SWCNTs-modified electrochemical interface.

SWCNTs have been previously demonstrated to promote the electron transfer kinetics of ascorbate electro-oxidation at a decreased over-potential and possess a strong ability against

^a Beijing National Laboratory for Molecular Sciences, CAS Key Laboratory of Analytical Chemistry for Living Biosystems, Institute of Chemistry, Chinese Academy of Sciences, Beijing 100190, China. E-mail: fuyi.wang@iccas.ac.cn

^b College of Chemistry, Beijing Normal University, Beijing 100875, China

^c University of Chinese Academy of Sciences, Beijing 100049, China

† Electronic supplementary information (ESI) available. See DOI: <https://doi.org/10.1039/d3cc01818k>



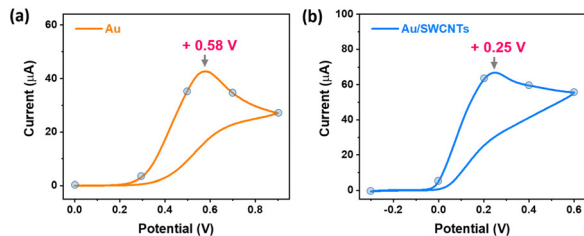


Fig. 1 Cyclic voltammograms (CVs) obtained at the gold film electrodes without (a) and with (b) modification with SWCNTs in phosphate buffer (pH 7.0) containing ascorbate in fabricated microfluidic electrochemical devices. We chose the values of step potentials as shown by the dots on the CV curves during the anodic scan for conducting further *in situ* liquid SIMS measurements.

electrode surface fouling.¹ To evaluate the performance of SWCNTs within our fabricated vacuum-compatible electrochemical devices, we used the gold film working electrode without or with modification of SWCNTs in the respective devices for a comparative study. The SEM image of the SWCNTs was shown in Fig S1 (ESI[†]). Fig. 1 and Fig. S2 (ESI[†]) presents the obtained cyclic voltammograms (CVs) in a 10 mM sodium phosphate buffer (pH 7.0) in the absence (Fig. S2, ESI[†]) or presence (Fig. 1) of ascorbate. In the control case of using the Au working electrode, it was obvious that the electro-oxidation of ascorbate occurred with a high peak potential value of +0.58 V (Fig. 1a). If using the SWCNTs-modified Au (briefed as Au/SWCNTs) electrode, the peak oxidation potential value in presence of ascorbate significantly shifted negatively to +0.25 V (Fig. 1b). The lowered oxidation potential of ascorbate suggested a faster reaction kinetics endowed by the SWCNTs, being similar to previous results.¹ In our recent report, we unraveled that the gold electrode surface in a phosphate buffer suffered from formation of a compact adsorption phase, which seriously retarded the ascorbate electro-oxidation.²⁵ Therefore, we propose that the improved electrochemical performance towards the ascorbate oxidation may be attributed to the altered interfacial chemistry by SWCNTs modification.

Next, we introduced the fabricated high vacuum-compatible electrochemical devices into the SIMS analysis chamber, and performed the electrochemical liquid SIMS measurements to *in situ* probe the interfacial chemistry in absence or presence of SWCNTs in *operando* conditions as illustrated in Fig. 2 and Fig. S3 (ESI[†]). We first describe the dynamic analysis process in the control case of using the Au nanofilm electrode as shown in Fig. S3 (ESI[†]). During the initial stage, the primary ion beam scanned on a small round area of 2 µm in diameter of the SiN membrane window (Fig. S3a, ESI[†]). As soon as the membrane was drilled through, a tiny aperture was created as indicated by the sharp decline in the SiN⁻ ion signal (Fig. S3b, ESI[†]). At this time point, the Au⁻ ion signal and the representative electrolyte-related signals of OH⁻ and PO₂⁻ also instantly increased (Fig. S3c, ESI[†]), revealing the permeation of the electrolyte to the SiN/Au interface through the porous granular structure of the sputter-deposited nanofilm electrode.^{24,29} The penetration of the electrolyte is a continuous process due to the

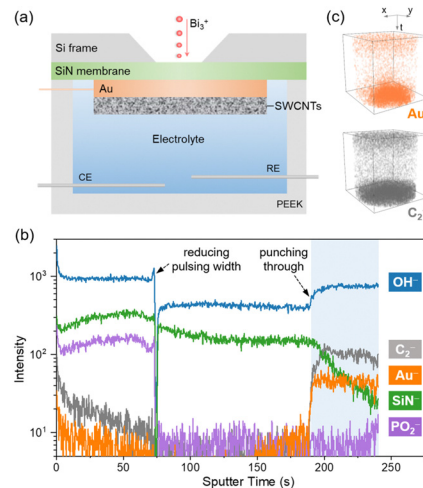


Fig. 2 (a) Schematic illustration of the side view of a fabricated electrochemical device for *in situ* liquid SIMS analysis. (b) The representative dynamic SIMS depth profiles in the negative ion mode for analysis of Au/SWCNTs–electrolyte interface when applying a potential of 0 V to the working electrode. The phosphate buffer in the absence of ascorbate was used as the electrolyte. The signals of Au⁻ (for Au electrode), C₂⁻ (for SWCNTs), and OH⁻ (for electrolyte) signals appeared immediately when the SiN membrane was drilled through by the primary ions, reflecting the permeation of electrolyte through the Au/SWCNTs composite layer as illustrated in Fig. S4 and S5 (ESI[†]). The highlighted time region in blue refers to the stage where the primary ions bombard the Au/SWCNTs–electrolyte interface. (c) The corresponding 3D chemical mapping of Au⁻ and C₂⁻ during the analysis.

pressure inside, resulting in the formation of a renewable thin electrolyte layer on the Au electrode surface and allowing the successful *operando* probing of the Au–electrolyte interfacial chemistry (Fig. S3b, ESI[†]). If the Au film electrode surface was modified with a layer of SWCNTs (Fig. 2a), surprisingly the characteristic ions of the Au nanofilm (Au⁻), the SWCNTs film (C₂⁻), and the electrolyte (OH⁻) were all immediately detected following the sputtering through of the SiN membrane and showed relatively stable signal trends afterwards (Fig. 2b). The simultaneous detection of the Au- and SWCNTs-related signals indicated the unexpected co-existing of these two species right beneath the SiN membrane. A plausible explanation is that during the SWCNTs film preparation process the SWCNTs dispersion on the electrode surface may infiltrate into the porous Au nanofilm layer when slowly drying in air, resulting in the formation of Au/SWCNTs composite layer structure besides the SWCNTs film (Fig. S4, ESI[†]). During the *in situ* liquid SIMS probing, the instant climbing of OH⁻ signal after a hole was created on the SiN membrane indicated that the electrolyte could first permeate through the SWCNTs film and then the Au/SWCNTs composite film to reach the bottom edge of the detection hole, allowing the detection of the Au/SWCNTs–electrolyte interfacial chemistry (Fig. S5, ESI[†]).

Then, we reconstructed the mass spectra (Fig. 3 and Fig. S6, ESI[†]) and 2D chemical mapping (Fig. S7 and S8, ESI[†]) from the time region of relatively stable interface-related signals in the depth profiles (Fig. 2b and Fig. S3c, ESI[†]) to investigate whether and how the interfacial chemistry in phosphate buffer was



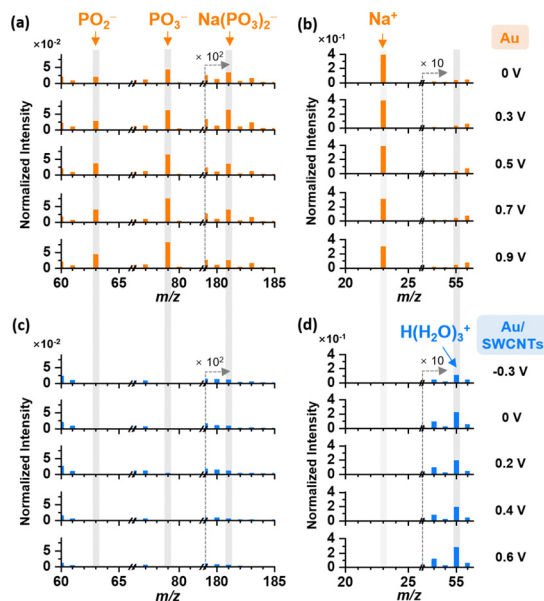


Fig. 3 Representative normalized SIMS spectra in the negative (a and c) and positive (b and d) modes, respectively, revealing the different chemical structures of the electrical double layers at different electrode–electrolyte interfaces in phosphate buffer using the gold film electrode without (a and b) or with (c and d) modification of SWCNTs.

altered by the modification of SWCNTs. In the control case of using the gold film electrode, we detected obvious signals of PO_2^- at m/z 63 and PO_3^- at m/z 79 in the negative ion mode, which were characteristic fragment ions of H_2PO_4^- and HPO_4^{2-} (Fig. 3a and Fig. S7a, ESI†). The signal trends of these two ions showed an increase with elevating the potential in the anodic direction (Fig. S9, ESI†). This is because the higher the electrode potential, the larger the number of negatively charged anions were electrostatically attracted onto the electrode surface, forming an anion-rich Stern layer. Besides, we also observed the abnormally strong Na^+ ion signal at m/z 23 in the positive ion mode (Fig. 3b and Fig. S8a, ESI†). Cations were predicted by the classic double layer theory to be repulsed from the positively charged electrode surface by Coulombic force. However, in our recent report,²⁵ Na^+ cations were identified to co-exist with phosphate anions in the Stern layer through formation of compact cation–anion ion pairs, which could stabilize the adsorption phase of crowded phosphate anions on the gold surface. This conclusion was further demonstrated by the obvious $\text{Na}(\text{PO}_3)_2^-$ ion at m/z 181 detected in the negative ion mode in this work (Fig. 3a and Fig. S7a, ESI†). It is worthy to note that the trend of Na^+ cations presented a complex potential-dependence during dynamic potential scanning, reflecting fine structures of the electrical double layer.²⁵ The signals of Na^+ and $\text{Na}(\text{PO}_3)_2^-$ ions in this work also showed variance with changing the potential. However, due to the relatively large interval of the measured step potentials we do not focus on describing fine characteristics of the signal trends here but compare the chemical difference between the two kinds of electrochemical interfaces instead. In sharp contrast to the control case, after modifying the electrode with SWCNTs we

barely detected signals of PO_2^- , PO_3^- , Na^+ or $\text{Na}(\text{PO}_3)_2^-$ (Fig. 3c, d and Fig. S7b, S8b, ESI†), showing that the formation of adsorption phase was avoided at the Au/SWCNTs–electrolyte interface. Therefore, reaction sites at the interface were well-preserved to be unoccupied for the access of electrochemically reactive ion species, which should account for the facilitated electron transfer process during the ascorbate electro-oxidation.

To further strengthen that the above information actually came from the interfaces, we presented the direct molecular ions of the interfacial chemistry including AuHPO_2^- at m/z 261, and $\text{AuNaH}_2\text{PO}_4^-$ at m/z 317 in Fig. S6 (ESI†). The obvious AuHPO_2^- ion signal was the straightforward evidence of the accumulation of phosphate anions at the gold electrode surface and that of the $\text{AuNaH}_2\text{PO}_4^-$ ion demonstrated that Na^+ cations indeed were anchored at the surface through compact cation–anion interactions (Fig. S6a, ESI†). These two signals disappeared at the Au/SWCNTs–electrolyte interface (Fig. S6b, ESI†), which unambiguously supported the aforementioned conclusion that the modification of the gold electrode surface by SWCNTs fundamentally tuned the interfacial chemistry to be free of the dense adsorption phase.

Moreover, at the Au–electrolyte interface the $\text{H}(\text{H}_2\text{O})_3^+$ ion signal at m/z 55, which has been identified as the dominant form of protonated water cluster ions,^{22,28} was very weak (Fig. 3b and Fig. S8a, ESI†). This indicated the limited existence of water molecules at the interface, which was possibly due to the dense network-like structure of adsorption phase knitted by compact cation–anion interactions. In comparison, the apparent $\text{H}(\text{H}_2\text{O})_3^+$ ion signal (Fig. 3d and Fig. S8b, ESI†) at the Au/SWCNTs–electrolyte interface indicated the abundance of surface water molecules. The electro-oxidation of ascorbate has been evidenced in our previous reports to be a typical proton coupled electrochemical reaction which involves the releasing of one proton from ascorbate accompanied by two electrons entering an electrode.^{21,25} Water molecules could act as a potential proton acceptor. We recently observed the recombination of the released protons in the oxidation process with surrounding water molecules at electrode–electrolyte interfaces to complete the proton transfer process.²² Therefore, the abundance of water molecules at the interface upon the SWCNTs modification may promote the proton coupled electrochemical oxidation of ascorbate.

Furthermore, we *in situ* explored the influence of the altered interfacial chemistry on the electrochemical oxidation reaction of ascorbate as shown in Fig. 4. At the Au–electrolyte interface, we detected the obvious ascorbate ion signal $\text{C}_6\text{H}_7\text{O}_6^-$ at m/z 175 (Fig. 4a) in comparison with the background signal (Fig. S10a, ESI†), indicating the electrochemically adsorption of ascorbate ions onto the interface. Besides, we also successfully obtained the ion signals of the oxidation intermediate $\text{C}_6\text{H}_6\text{O}_6^-$ at m/z 174 and oxidation product $\text{C}_6\text{H}_5\text{O}_6^-$ at m/z 173 (Fig. 4a), which showed a clear increase with elevating the oxidation potential. The observations were in accordance with our previous reports,^{21,25} demonstrating the proton coupled electron transfer reaction mechanism (Fig. 4c). At the SWCNTs modified interface, the main difference is the appearance of the ion peak at m/z 193 (Fig. 4b). The ion was not related to the SWCNTs as it was barely observed at the Au/SWCNTs–electrolyte



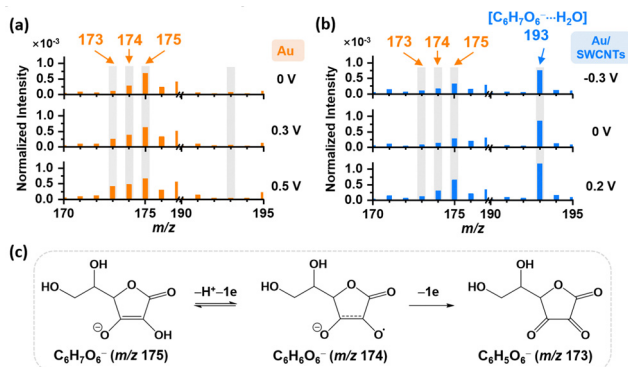


Fig. 4 (a) and (b) Negative ion SIMS spectra of ascorbate-related ions detected at the electrochemical interface in phosphate buffer containing ascorbate using the gold film before (a) or after (b) modification with SWCNTs as the working electrode. (c) Schematic diagram of the electro-oxidation reaction pathway of ascorbate.

interface in the absence of ascorbate (Fig. S10b and S11, ESI[†]). Instead, it was ascribed to the hydrated ascorbate ion [C₆H₇O₆⁻·H₂O], further demonstrating the abundance of water molecules at the SWCNTs modified interface. The water molecule within the hydrated ion structure may act as a proton acceptor to facilitate the proton transfer process during the electro-oxidation of ascorbate. Due to the adduct ion formation between the ascorbate and a water molecule, the signal intensity of the bare ascorbate ion C₆H₇O₆⁻ at m/z 175 (Fig. 4b) is relatively weaker than that at the interface without SWCNTs modification (Fig. 4a). Apart from the ascorbate-related ions, we also observed the formation of the electro-oxidation intermediate C₆H₆O₆⁻ (m/z 174) at the SWCNTs modified interface as its signal increased obviously at a high oxidation potential of 0.2 V (Fig. 4b) similarly to the observation in the situation without SWCNTs (Fig. 4a). However, the product ion signal C₆H₅O₆⁻ at m/z 173 was nearly undetected at the interface with SWCNTs modification (Fig. 4b). A plausible explanation is that the product was rapidly excluded from the SWCNTs modified interface and diffused into the bulk upon its formation during electro-oxidation. This observation supported the previous conclusion derived from the stable amperometric response in a continuous flow system¹ that the SWCNTs-modified electrode surface was protected from adsorption of the ascorbate oxidation product and thus exhibited a strong ability against electrode fouling.

In conclusion, we present the first *in situ* molecular observation of the chemistry at the interface between a SWCNTs-modified gold electrode surface and a phosphate buffer electrolyte using our tailored electrochemical liquid SIMS platform. We unravel that in comparison with the gold electrode–electrolyte interface the modification of SWCNTs at the interface altered the interfacial structures to be free of a dense adsorption layer and more abundant in water molecules, which promoted both the facilitated electron transfer and proton transfer of the electro-oxidation reaction of ascorbate. We envision that such a fundamental understanding of the interfacial chemistry will provide constructive insights to guide future engineering of electrochemical interfaces for applications such as energy conversion and storage, electrocatalysis, and biosensing.

We acknowledge financial support from the National Natural Science Foundation of China (Grants No. 21904128, 21927804).

Conflicts of interest

There are no conflicts to declare.

Notes and references

- 1 M. Zhang, K. Liu, K. Gong, L. Su, Y. Chen and L. Mao, *Anal. Chem.*, 2005, **77**, 6234–6242.
- 2 F. Wu, L. Su, P. Yu and L. Mao, *J. Am. Chem. Soc.*, 2017, **139**, 1565–1574.
- 3 Z. Yang, J. Tian, Z. Yin, C. Cui, W. Qian and F. Wei, *Carbon*, 2019, **141**, 467–480.
- 4 P. Simon and Y. Gogotsi, *Acc. Chem. Res.*, 2013, **46**, 1094–1103.
- 5 Y. Liang, H. Wang, P. Diao, W. Chang, G. Hong, Y. Li, M. Gong, L. Xie, J. Zhou, J. Wang, T. Z. Regier, F. Wei and H. Dai, *J. Am. Chem. Soc.*, 2012, **134**, 15849–15857.
- 6 C. Wang, M. Waje, X. Wang, J. M. Tang, R. C. Haddon and Y. Yan, *Nano Lett.*, 2004, **4**, 345–348.
- 7 Z. Wang, M. Zhang, W. Ma, J. Zhu and W. Song, *Small*, 2021, **17**, 2100219.
- 8 J. Deng, P. Ren, D. Deng and X. Bao, *Angew. Chem., Int. Ed.*, 2015, **54**, 2100–2104.
- 9 Y. Shao, J. Wang, H. Wu, J. Liu, I. A. Aksay and Y. Lin, *Electroanalysis*, 2010, **22**, 1027–1036.
- 10 S. Guo, P. Yu, W. Li, Y. Yi, F. Wu and L. Mao, *J. Am. Chem. Soc.*, 2020, **142**, 2074–2082.
- 11 J. Li, X. Gao, B. Liu, Q. Feng, X.-B. Li, M.-Y. Huang, Z. Liu, J. Zhang, C.-H. Tung and L.-Z. Wu, *J. Am. Chem. Soc.*, 2016, **138**, 3954–3957.
- 12 C. Hu, H. Liu, Y. Liu, J.-F. Chen, Y. Li and L. Dai, *Nano Energy*, 2019, **63**, 103874.
- 13 J. Li, X. Gao, X. Jiang, X.-B. Li, Z. Liu, J. Zhang, C.-H. Tung and L.-Z. Wu, *ACS Catal.*, 2017, **7**, 5209–5213.
- 14 C. Huang, S. Zhang, H. Liu, Y. Li, G. Cui and Y. Li, *Nano Energy*, 2015, **11**, 481–489.
- 15 Y. Xue, J. Li, Z. Xue, Y. Li, H. Liu, D. Li, W. Yang and Y. Li, *ACS Appl. Mater. Interfaces*, 2016, **8**, 31083–31091.
- 16 X. Gao, J. Li, R. Du, J. Zhou, M.-Y. Huang, R. Liu, J. Li, Z. Xie, L.-Z. Wu, Z. Liu and J. Zhang, *Adv. Mater.*, 2017, **29**, 1605308.
- 17 A. M. Appel and M. L. Helm, *ACS Catal.*, 2014, **4**, 630–633.
- 18 O. M. Magnussen and A. Groß, *J. Am. Chem. Soc.*, 2019, **141**, 4777–4790.
- 19 J. P. Kraack and P. Hamm, *Chem. Rev.*, 2017, **117**, 10623–10664.
- 20 J.-F. Li, Y.-J. Zhang, S.-Y. Ding, R. Panneerselvam and Z.-Q. Tian, *Chem. Rev.*, 2017, **117**, 5002–5069.
- 21 Z. Wang, Y. Zhang, B. Liu, K. Wu, S. Thevuthasan, D. R. Baer, Z. Zhu, X.-Y. Yu and F. Wang, *Anal. Chem.*, 2017, **89**, 960–965.
- 22 J.-G. Wang, Y. Zhang, X. Yu, X. Hua, F. Wang, Y.-T. Long and Z. Zhu, *J. Phys. Chem. Lett.*, 2019, **10**, 251–258.
- 23 Y. Zhang, J.-G. Wang, X. Yu, D. R. Baer, Y. Zhao, L. Mao, F. Wang and Z. Zhu, *ACS Energy Lett.*, 2019, **4**, 215–221.
- 24 Y. Zhou, M. Su, X. Yu, Y. Zhang, J.-G. Wang, X. Ren, R. Cao, W. Xu, D. R. Baer, Y. Du, O. Borodin, Y. Wang, X.-L. Wang, K. Xu, Z. Xu, C. Wang and Z. Zhu, *Nat. Nanotechnol.*, 2020, **15**, 224–230.
- 25 Y. Zhang, J. Tang, Z. Ni, Y. Zhao, F. Jia, Q. Luo, L. Mao, Z. Zhu and F. Wang, *J. Phys. Chem. Lett.*, 2021, **12**, 5279–5285.
- 26 Y. Zhang, W. Zeng, L. Huang, W. Liu, E. Jia, Y. Zhao, F. Wang and Z. Zhu, *Anal. Chem.*, 2019, **91**, 7039–7046.
- 27 Y. Zhang, Z. Xing, B. Fan, Z. Ni, F. Wang, X. Hu and Y. Chen, *Angew. Chem., Int. Ed.*, 2023, **62**, e202215799.
- 28 Y. Zhang, M. Su, X. Yu, Y. Zhou, J. Wang, R. Cao, W. Xu, C. Wang, D. R. Baer, O. Borodin, K. Xu, Y. Wang, X.-L. Wang, Z. Xu, F. Wang and Z. Zhu, *Anal. Chem.*, 2018, **90**, 3341–3348.
- 29 Z. Zhu, Y. Zhou, P. Yan, R. S. Vemuri, W. Xu, R. Zhao, X. Wang, S. Thevuthasan, D. R. Baer and C.-M. Wang, *Nano Lett.*, 2015, **15**, 6170–6176.

